22nd Australasian Fluid Mechanics Conference AFMC2020
Brisbane, Australia, 7–10 December 2020
https://doi.org/10.14264/3962085

Control of Cloud Cavitation through Microbubbles

J. A. Venning[1], **B. W. Pearce**[1] **and P. A. Brandner**[1]

[1] University of Tasmania, Launceston, Tasmania, 7250, Australia

Abstract

The dynamics of cloud cavitation about a 3D hydrofoil are investigated experimentally in a cavitation tunnel with deplete, sparse and abundant freestream nuclei populations. The rectangular-planform, NACA 0015 hydrofoil was tested at a Reynolds number of 1.4×10^6, an incidence of $6°$ and a cavitation number of 0.55. High-speed photography of cavitation shedding phenomena was acquired simultaneously with unsteady force measurement to enable identification of cavity shedding modes corresponding with force spectral peaks. Nuclei populations were varied through the injection of polydisperse microbubbles. Both the deplete and abundant cases were characterised by large-scale cloud cavitation. For a sparsely seeded flow, however, coherent fluctuations are significantly reduced due to random nuclei activation and cavity breakup resulting in minimum relative unsteady lift.

Keywords
Cavitation; multi-phase flow;.

Introduction

The periodic formation, growth, detachment and advection of partial cavities is termed cloud cavitation. This phenomenon is associated with performance degradation, erosion and unsteady loads with resultant vibration, noise, and fatigue. Two mechanisms have been found to drive this instability: a re-entrant liquid jet and a condensation shockwave. Details on the re-entrant jet are given in [8, 5, 12]. Cavities become susceptible to condensation shockwaves as the speed of sound reduces in bubble flows [6]. This mechanism tends to become more dominant at lower cavitation numbers [1, 16].

The dynamics and inception of cavitation are controlled not only by the geometry and flow parameters, but also by the quality of the water. Water is known to be able to withstand extreme negative pressures (tensions) without rupturing, for example 28 MPa in [4], although typical tensions are $O(-10\,\text{kPa})$. As such, the cavitation index at inception is generally lower than the minimum pressure coefficient in the flow, since some tension needs to be applied to the water before it ruptures. This required tension is related to the strength of microbubbles, solid contaminants, and micro-organisms in the flow, which provide nuclei for cavitation. The quantity and strength of these nuclei can be measured directly using a cavitation susceptibility meter [18], and for many flows, these nuclei can be regarded as inactive after the initial inception. [3] showed the cavitation behaviour of a hydrofoil to be dependent on the quality of the water. An unseeded cavitation pattern is usually described by a clearly defined detachment line downstream of a laminar seperation bubble [7]. When additional microbubbles are included, the state changes to 'traveling bubble' cavitation, where individual bubbles are activated as they encounter lower pressures. The boundary layer is destabilised [11], and it no longer separates.

Some elements of the flow about a NACA 0015 hydrofoil have been described earlier [19, 17], and here we extend this work to look at the effect of a sparse nuclei concentration on the cavitation behaviour. This work is fully described in [20].

Experimental setup

Experiments were carried out in the Cavitation Research Laboratory (CRL) variable-pressure water tunnel at the University of Tasmania (figure 1). The tunnel test section (figure 1) is 0.6 m square by 2.6 m long in which the operating velocity and absolute pressure ranges are 2 to 13 m/s and 4 to 400 kPa, respectively. The tunnel volume is $365\,\text{m}^3$ with demineralised water as the working fluid. The CRL tunnel has ancillary systems for rapid degassing and for continuous injection and removal of cavitation nuclei and large volumes of incondensable gas (additional description is in [2]).

The model hydrofoil, of anodised aluminium, has a rectangular planform of 0.3 m span (b) and 0.15 m chord (c) with constant NACA 0015 section and a faired tip. The model is mounted vertically from the test section ceiling on a 6-component force balance [21] for dynamic force measurement at an acquisition rate of 1 kHz. The lift and drag coefficients are $C_\text{L} = L/qbc$ and $C_\text{D} = D/qbc$, respectively, where L is the lift force, D is the drag force and q is the freestream dynamic pressure.

The Reynolds number (Re, based on chord length) was constant at 1.4×10^6 with the hydrofoil set at a fixed incidence of $6°$. The cavitation number was fixed at 0.55 and is defined as $\sigma = (p_\infty - p_\text{v})/q$, where p_∞ is the static pressure at the test section centreline and p_v is the vapour pressure.

Simultaneous measurements were made of the hydrofoil lift

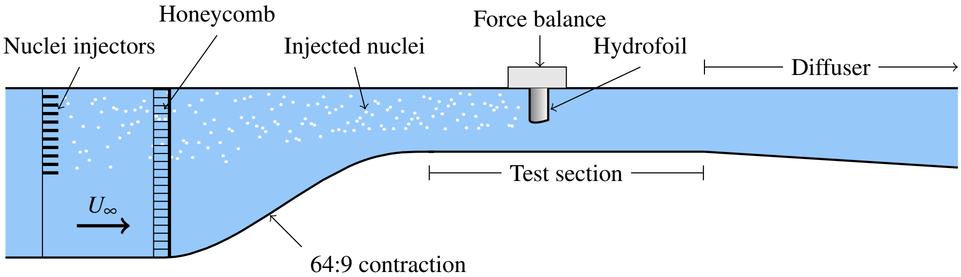

Figure 1. Tunnel schematic showing the experimental layout including the microbubble nuclei injection, contraction, test section, and diffuser.

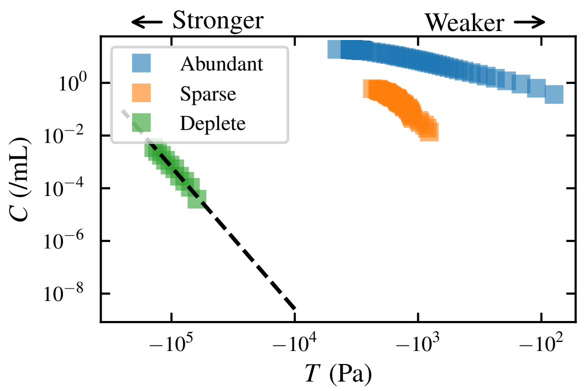

Figure 2. Tension measurements for the three different nuclei populations investigated.

force and high-speed photography of cavitation taken from the side of the test section, normal to the flow direction. The high-speed photography was recorded using a LaVision HighSpeed-Star8 camera at a spatial resolution of 1024×1024 pixels using a Nikkor f/1.4 50 mm lens. Simultaneous forces and high-speed images were recorded at 7 kHz for 3 s. Long-time series measurements of force for obtaining high-resolution spectra were recorded at 1 kHz for 240 s giving about 5,000 cycles of the dominant frequency.

Various seeding conditions were investigated where the freestream flow ranged from being deplete of active nuclei through to that with an abundance of microbubble nuclei. For the deplete case no nuclei are injected such that only the natural population is present in the tunnel water which do not provide active nuclei in the freestream for this flow condition [18, 10, 9]. For the nucleated cases, poly-disperse microbubbles are injected upstream of the honeycomb, as shown in figure 1. An array of injectors were installed over a sufficient area to seed the streamtube that flows about the hydrofoil. Mie-scattering imaging (MSI) measurements of the bubble population were performed [13, 14] and are given in figure 2. In all seeding cases the tunnel water was maintained at a dissolved oxygen level of 3 ppm.

Results

Photographs of the cavitation appearance in figure 3 show the effect of the additional nuclei on the cavitation for otherwise identical conditions. In (a), the near-straight leading edge of the cavity indicates the presence of the laminar separation bubble upstream. This is the classical 'attached' cavitation, with a large re-entrant jet forming underneath the cavity, and a large-scale cloud cavity being shed. For the abundant case (c), the leading-edge cells have now disappeared, being replaced by travelling bubble cavitation. These are the individual injected nuclei being activated as they encounter the low-pressure zone near the leading edge. The growth of these cavities is stunted due to the lack of available space [15]. Continual feeding of these nuclei into the trailing vortex region fill this area with gas. In the intermediate case, (b), some travelling microbubbles are seen, and some areas with attached cavitation. The size of the cloud cavities are reduced from $0.5b$ to a maximum of $0.2b$, and many different wavelengths are evident in the image. The microbubbles that are activated grow to a larger size than the abundant case, and wash away any attached cavities in the vicinity. A transition to turbulent flow is evident in the liquid film beneath the large bubble near the tip of the hydrofoil.

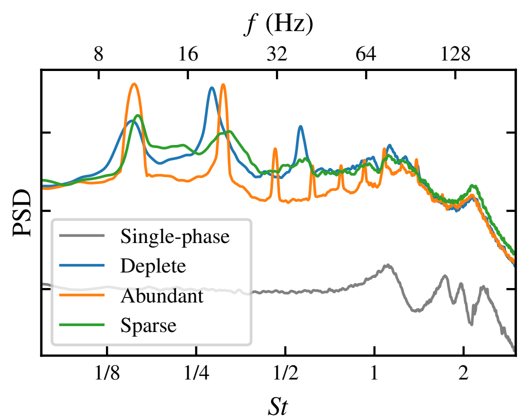

Figure 4. Lift force spectra showing the influence of additional nuclei on the unsteady forces. The vertical scale is base-10 logarithmic.

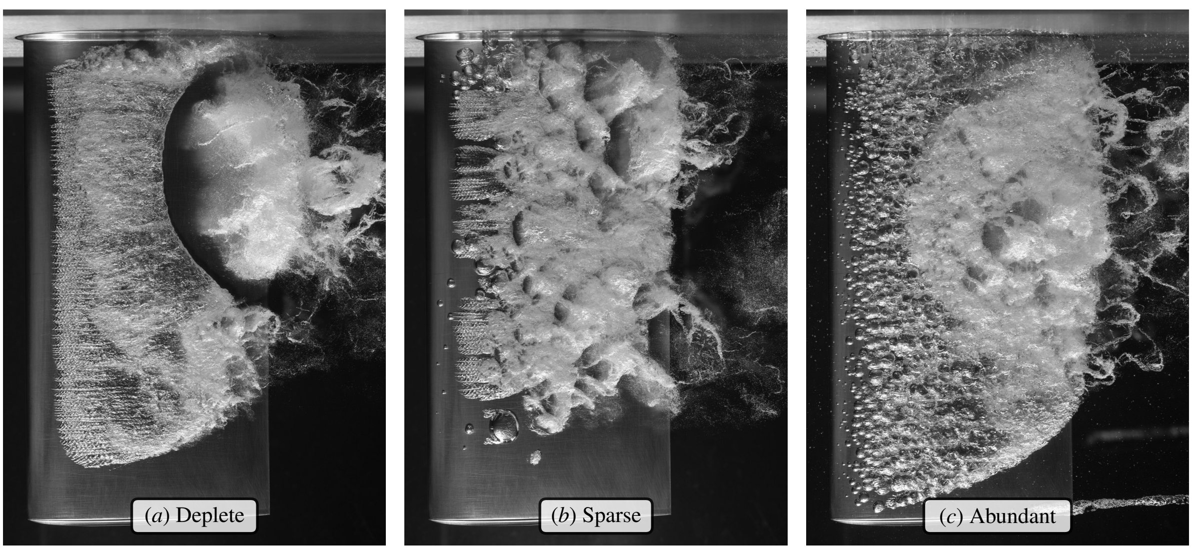

Figure 3. Photographs of the cavity for the three densities of nuclei. The flow conditions are identical between the three cases with a Reynolds number of 1.5×10^6, a cavitation number of 0.55, and an incidence of $6°$.

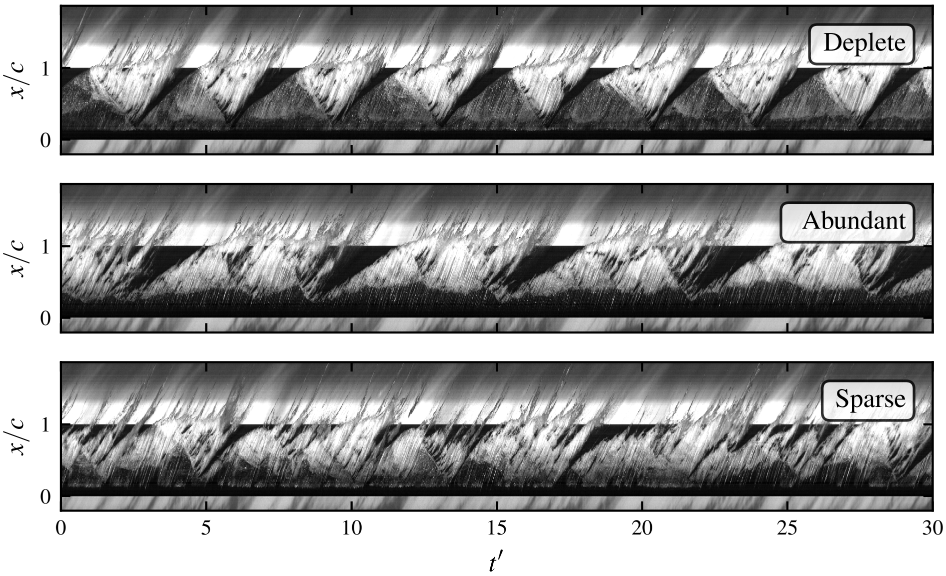

Figure 5. Comparison of streamwise space-time diagrams at half-span for the three seeding conditions. The flow is from bottom to top. The periodic shedding of cavity clouds in the Deplete and Abundant cases has been replaced by aperiodic shedding in the Sparse case.

Seeding	C_L	C'_L
Deplete	0.354	0.064
Dense	0.283	0.061
Sparse	0.353	0.047

Table 1. Steady and unsteady lift coefficients for the three seeding densities.

Figure 4 shows spectra of the lift force for each of the three conditions. The single-phase spectrum is provided as a reference regarding the force balance and hydrofoil natural frequencies. The unsteadiness from cavitation is an order of magnitude higher than what is generated from turbulence alone. For the deplete case, the primary shedding freqency is $St = 0.28$. With abundant seeding, the peak frequency reduces by a factor of 1.8 to $St = 0.15$. A secondary harmonic peak is evident related to the passage of two shockwaves per shedding cycle. The first shockwave does not cause complete condensation, while the second one is stronger. These details are shown in the space-time diagrams discussed below. For the sparse level of seeding, the spectral content in each peak is reduced. The intermittent and sparsely activated microbubbles break up the development of large-scale coherent structures which are responsible for the unsteady forces.

Space-time diagrams for the three cases are in figure 5, generated from a slice of the high-speed video at $z/b = 0.5$. Flow is from the bottom to the top, and the hydrofoil extends from $x/c = 0$ to $x/c = 1$. For the deplete case, a cycle is defined by the growth of a cavity, and the generation of a condensing shockwave once the cavity reaches the trailing edge. The propagation of this schockwave condenses the cavity and the cycle repeats. With abundant seeding, the growth cycle is slowed down considerably. The two shockwaves are evident, the first of which preconditions the cavity to the second, stronger, shockwave, which condenses a larger portion of the cavity. For the third case, the coherence and repeatability of the shedding mechanism is no longer seen, highlighting how variable the cavitation size and therefore force fluctuations are.

The steady and fluctuating lift coefficients are given in table 1 for the three cases, showing the reduction in unsteadiness that is achievable with nuclei control. This reduction comes with no substantial loss of the lift force, showing that the hydrofoil efficiency is maintained. This technique could be used for alleviating the adverse effects of cavitation such as fatigue loading.

Conclusions

The dynamics of cloud cavitation about a hydrofoil have been shown to be dependent on the nuclei levels in the water. The mechanisms that lead to instability and cavity shedding vary according to the nuclei content of the water, which was varied from essentially no active freestream nuclei to an abundant case with a high concentration of active nuclei. The spectral content of the lift force was dramatically reduced when a sparse concentration of microbubbles was added to the flow.

Acknowledgements

The authors sincerely thank Dr. Dean Giosio and Dr. Samuel Smith for their assistance in acquiring the data and Mr. Steve Kent and Mr. Robert Wrigley for assistance setting up the experiments.

References

[1] Arndt, R. E., Song, C., Kjeldsen, M., He, J. and Keller, A., Instability of partial cavitation: a numerical/experimental approach, in *Twenty-Third Symposium on Naval Hydrodynamics, Val de Reuil, France*, National Academies Press, 2000.

[2] Brandner, P. A., Lecoffre, Y. and Walker, G. J., Development of an Australian National Facility for Cavitation Research, in *Sixth International Symposium on Cavitation*, 2006, 1–9, 1–9.

[3] Briancon-Marjollet, Franc, J.-P. and Michel, J. M., Transient bubbles interacting with an attached cavity and the boundary layer, *Journal of Fluid Mechanics*, **218**, 1990, 355–376.

[4] Briggs, L. J., Limiting negative pressure of water, *Journal of Applied Physics*, **21**, 1950, 721–722.

[5] Callenaere, M., Franc, J. P., Michel, J. M. and Riondet, M., The cavitation instability induced by the development of a re-entrant jet, *Journal of Fluid Mechanics*, **444**, 2001, 223–256.

[6] Crespo, A., Sound and shock waves in liquids containing bubbles, *The Physics of Fluids*, **12**, 1969, 2274–2282.

[7] Franc, J. P. and Michel, J. M., Attached cavitation and the boundary layer: Experimental investigation and numerical treatment, *Journal of Fluid Mechanics*, **154**, 1985, 63–90.

[8] Kawanami, Y., Kato, H., Yamaguchi, H., Tanimura, M. and Tagaya, Y., Mechanism and Control of Cloud Cavitation, *ASME Journal of Fluid Engineering*, **119**, 1997, 788–794.

[9] Khoo, M. T., Venning, J. A., Pearce, B. W., Brandner, P. A. and Lecoffre, Y., Development of a Cavitation Susceptibility Meter for Nuclei Size Distribution Measurements, in *20th Australasian Fluid Mechanics Conference*, 2016.

[10] Khoo, M. T., Venning, J. A., Pearce, B. W., Takahashi, K., Mori, T. and Brandner, P. A., Natural nuclei population dynamics in cavitation tunnels, *Experiments in Fluids*, **61**.

[11] Li, C.-Y. and Ceccio, S. L., Interaction of single travelling bubbles with the boundary layer and attached cavitation, *Journal of Fluid Mechanics*, **322**, 1996, 329–353.

[12] Pelz, P., Keil, T. and Groß, T., The transition from sheet to cloud cavitation, *Journal of Fluid Mechanics*, **817**, 2017, 439–454.

[13] Russell, P., Venning, J., Pearce, B. W. and Brandner, P. A., Calibration of Mie scattering imaging for microbubble measurement in hydrodynamic test facilities, *Experiments in Fluids*, **61**, 2020, 1–17.

[14] Russell, P. S., Barbaca, L., Venning, J. A., Pearce, B. W. and Brandner, P. A., Measurement of nuclei seeding in hydrodynamic test facilities, *Experiments in Fluids*, **61**.

[15] Russell, P. S., Venning, J. A., Brandner, P. A., Pearce, B. W., Giosio, D. R. and Ceccio, S. L., Microbubble disperse flow about a lifting surface, in *32nd Symposium on Naval Hydrodynamics*, 2018.

[16] Smith, S. M., Venning, J. A., Pearce, B. W., Young, Y. L. and Brandner, P. A., The influence of fluid-structure interaction on cloud cavitation about a stiff hydrofoil. part 1., *Journal of Fluid Mechanics*, **896**, 2020, A1.

[17] Venning, J., Giosio, D., Smith, S., Pearce, B. and Brandner, P., The Influence of Nucleation on the Spectral Content of Cloud Cavitation About a Hydrofoil, in *Proceedings of the 10th International Symposium on Cavitation (CAV2018)*, Baltimore, 2018, 1025–1030, 1025–1030.

[18] Venning, J., Khoo, M., Pearce, B. and Brandner, P., Background nuclei measurements and implications for cavitation inception in hydrodynamic test facilities, *Experiments in Fluids*, **59**, 2018, 71.

[19] Venning, J., Smith, S., Brandner, P., Giosio, D. and Pearce, B., The influence of nuclei content on cloud cavitation about a hydrofoil, in *Open Archives of the 17th International Symposium on Transport Phenomena and Dynamics of Rotating Machinery, ISROMAC 2017*, 2017, volume 2, 2–7, 2–7.

[20] Venning, J. A., Pearce, B. W. and Brandner, P. A., Nucleation effects on cloud cavitation about a hydrofoil, under consideration for publication in, *Journal of Fluid Mechanics*.

[21] Zarruk, G. A., Henderson, A. D., de Graaf, K. L., Brandner, P. A. and Pearce, B. W., Validation of a Microbubble Seeding Generator for Particle Image Velocimetry Applications, in *19th Australasian Fluid Mechanics Conference*, 2014.